Location prediction of electron TGFs

S. Xiong,[1] M. S. Briggs,[1] V. Connaughton,[1] G. J. Fishman,[2] D. Tierney,[3] G. Fitzpatrick,[3] S. Foley,[4] S. Guiriec,[1] R. H. Holzworth,[5] and M. L. Hutchins[5]

[1]   Terrestrial Gamma-ray Flashes (TGFs) are brief pulses of energetic radiation that correlate with thunderstorms and lightning. Most TGFs are observed as gamma-ray pulses; less frequently they can be observed as electrons and positrons that travel along the geomagnetic field line from the source to the detector. In this paper we predict where electron TGFs should be observed by tracing geomagnetic field lines from likely TGF sources and determining the intersections with satellite orbits. TGF source locations are based upon lightning maps by the Lightning Imaging Sensor (LIS) and the Optical Transient Detector (OTD). Predictions are made both for existing spacecraft with instruments observing TGFs and for other orbits. We compare the predictions to the locations of TGFs that have been observed as electron TGFs. 12 of the 13 known electron TGFs are within the predicted high-rate regions. Based on the predicted location maps of electron TGFs, we find that electron TGFs should sometimes be observed above areas with low lightning activity and that electron TGFs are best observed at low altitudes (below approximately 1000 km).

1.   Introduction

[2]   Terrestrial Gamma-ray Flashes (TGFs) are brief intense energetic emission from Earth's atmosphere. Since their unexpected discovery by the Burst And Transient Source Experiment (BATSE) on the Compton Gamma-Ray Observatory (CGRO) in the early 1990s [*Fishman et al.*, 1994], TGFs have been studied extensively with observations by the Reuven Ramaty High Energy Solar Spectroscopic Imager (RHESSI) [*Smith et al.*, 2005], the Astro-rivelatore Gamma a Immagini LEggero (AGILE) [*Marisaldi et al.*, 2010], and the Gamma-ray Burst Monitor (GBM) onboard the Fermi Gamma-ray Space Telescope (Fermi) [*Briggs et al.*, 2010; *Fishman et al.*, 2011]: They are featured with short duration (μs to ms), single pulse or multipulses and very hard spectrum (above 40 MeV) [*Briggs et al.*, 2010; *Marisaldi et al.*, 2010; *Tavani et al.*, 2011]; The association with thunderstorm regions [*Fishman et al.*, 1994] and lightning discharge [*Inan et al.*, 1996; *Cohen et al.*, 2006; *Cummer et al.*, 2005; *Connaughton et al.*, 2010] has been strongly confirmed; The widely accepted mechanism for explaining TGFs is Relativistic Runaway Electron Avalanche (RREA) [*Gurevich et al.*, 1992; *Roussel-Dupré and Gurevich*, 1996;

Lehtinen et al., 1999; *Dwyer*, 2003, 2007] in which electrons within intense electric fields are accelerated and produce secondaries by interacting with air leading to an avalanche of relativistic electrons and then gamma-ray photons through bremsstrahlung. The observed spectrum of TGFs follows a power law with an exponential cutoff at around 7 MeV, consistent with the RREA model [*Dwyer and Smith*, 2005]. However, recent AGILE observations of a high energy power law are inconsistent with this model [*Tavani et al.*, 2011].

[3]   *Lehtinen et al.* [2001] first suggested that the electron beams accompanying TGFs may escape upward from the hemisphere and then be indirectly detected through the interactions at the conjugate footprint, assuming those electron beams originate at high altitude above thunderstorms. However, spectral analysis of RHESSI data and accompanying modeling favor a low altitude (15–21 km) source [*Dwyer and Smith*, 2005; *Carlson et al.*, 2007]. Motivated by BATSE data, *Dwyer et al.* [2008] proposed a new mechanism to produce electron-positron beams: As the gamma-rays of TGFs propagate upwards through atmosphere, electrons and positrons are produced by Compton scattering and pair production. Although most electrons and positrons are quickly absorbed, a good fraction of these secondaries above 40 km can escape the atmosphere and travel along the geomagnetic field lines to be directly detectable by low-orbit satellites. Propagation effects give "electron TGFs" time histories that distinguish them from gamma-ray TGFs: arrival dispersion due to pitch angles causes longer durations, and if the magnetic field is stronger at the conjugate point there will be a second peak due to magnetic mirroring. Two factors change the detectability of electron TGFs compared to gamma-ray TGFs: first, gamma-rays disperse while the magnetic field confines the charged particles, which allows electron TGFs

[1]CSPAR, University of Alabama in Huntsville, Huntsville, Alabama, USA.
[2]Space Science Office, NASA Marshall Space Flight Center, Huntsville, Alabama, USA.
[3]School of Physics, University College Dublin, Dublin, Ireland.
[4]Max-Planck-Institut für Extraterrestrische Physik, Garching, Germany.
[5]Earth and Space Sciences, University of Washington, Seattle, Washington, USA.

to be detected at great distances from the sources. Second, because of the confinement of electrons within a narrow beam, the sample of known electron TGFs is much smaller than the gamma-ray TGF sample [*Dwyer et al.*, 2008; *Carlson et al.*, 2009].

[4] The first evidence of electron TGFs came from BATSE TGFs 2221 and 1470 [*Dwyer et al.*, 2008], as well as the RHESSI TGF of 17 January 2004 [*Smith et al.*, 2006], all of which showed long durations, while two of them, detected when the spacecrafts were over the Sahara desert but magnetically connected to active thunderstorm regions in southern Africa, contained a second pulse due to mirroring. Moreover, many possible electron TGFs have been identified from The Solar Anomalous Magnetospheric Particle Explorer (SAMPEX) Heavy Ion Large Telescope (HILT) [*Carlson et al.*, 2009], but can not be solidly confirmed due to the low time resolution (20 ms) of the data. As additional confirmation, the associated lightning discharge was observed for the first time at the footprint of the geomagnetic field line for an electron TGF (GBM TGF 100515) [*Cohen et al.*, 2010].

[5] Since its launch in June 2008, the Gamma-ray Burst Monitor (GBM) [*Meegan et al.*, 2009] onboard the Fermi has detected hundreds of TGFs by on-orbit trigger [*Briggs et al.*, 2010; *Fishman et al.*, 2011]. Most TGFs detected by GBM are gamma-ray events with duration usually less than 1 ms and usually between 0.05 ms and 0.20 ms. However, a few are identified as electron TGFs because they have long duration, lower maximum energy compared to most TGFs and lightning discharges suggesting storm activity at one of the termini of the geomagnetic field lines through Fermi but not underneath Fermi [*Briggs et al.*, 2010; *Connaughton et al.*, 2010; *Fishman et al.*, 2011]. Furthermore, the spectral analysis of three electron TGFs strongly confirmed that electron TGFs contains not only electrons but also positrons [*Briggs et al.*, 2011], as predicted by [*Dwyer et al.*, 2008].

[6] In this paper, we predict where electron TGFs should be observed by tracing geomagnetic field lines from likely TGF sources and determining the intersections with satellite orbits. In section 2, the TGF source locations and lightning maps are stated. In section 3, the geomagnetic field model and tracing method are presented. Predictions are made both for existing spacecraft with instruments observing TGFs and for other orbits, shown in section 4. We compare the predictions to the locations of TGFs that have been observed as electron TGFs and discuss the result in section 5.

2. TGF Location and Lightning Map

[7] Since TGFs have been conclusively associated with lightning discharge [*Inan et al.*, 1996; *Cohen et al.*, 2006; *Cummer et al.*, 2005; *Connaughton et al.*, 2010], and the geographic distribution of TGFs observed by RHESSI and AGILE are consistent with active lightning regions [*Smith et al.*, 2005; *Grefenstette et al.*, 2009; *Fuschino et al.*, 2011], the TGF occurrence rate is assumed to be proportional to the lightning rate so that lightning rate maps can be used to estimate the locations and rates of the TGF sources.

[8] We take use of the lightning data (available at http://ghrc.msfc.nasa.gov) observed by the Lightning Imaging Sensor (LIS) [*Christian et al.*, 1999] and Optical Transient Detector (OTD) [*Boccippio et al.*, 2000] from 1995 to 2005. We used the so-called "High resolution" maps which have the pixel size of 0.5 degree × 0.5 degree, and only consider the regions with flash rate greater than or equal to 10 flashes km^{-2} yr^{-1}. The full climatology (full year) and seasonal lightning maps used in this paper are shown in Figure 1.

[9] There is strong evidence that the TGF/lightning ratio varies geographically [*Smith et al.*, 2010; *Fuschino et al.*, 2011]. Since the TGF/lightning ratio directly determines the rate of electron TGFs in a geographical area, the geographic variation will change the relative importance of the regions where electron TGFs are favored. Therefore, we correct the dependence of TGF/lightning ratio on latitude and longitude by using the data given by *Smith et al.* [2010, Figures 6 and 7]. TGF/lightning ratio is calculated by dividing the RHESSI TGF numbers by the LIS/OTD lightning rates, corrected for the non-uniform RHESSI exposure. Then the trends with latitude and longitude are each fit with 4th order polynomial functions, see Figure 2.

[10] The TGF/lightning ratio calculated by this method is a relative value, so we can only calculate the relative rates of electron TGFs. The calculation of the absolute value from RHESSI data is unrealistic without the detection efficiency. Although there is an absolute estimation from AGILE observations [*Fuschino et al.*, 2011], that estimation is based on a very narrow latitude range so it may not extrapolate well to other regions.

3. Tracing Geomagnetic Field

[11] Since electrons will travel along the geomagnetic field lines, it can be determined where electron TGFs would be observed by an instrument in-orbit by calculating the intersections of geomagnetic field lines with the orbital plane.

[12] The International Geomagnetic Reference Field (IGRF) is a global model of the geomagnetic field of Earth. It is the standard mathematical description of the Earth's main magnetic field and its annual rate of change. Here the latest version of IGRF model, IGRF-11 [*Finlay et al.*, 2010], is used to describe geomagnetic field.

[13] As shown in Figure 3, the longitude and latitude of intersections are derived for source TGF for a given altitude of orbit. Note that there are usually two intersections for a particular field line and altitude, but there may be no intersection if the altitude is too high.

4. Locations of Electron TGFs

[14] For each pixel in the lightning map (see Figure 1) with flash rate greater than or equal to 10 flashes km^{-2} yr^{-1}, the central position of this pixel is taken as the location of the source TGF. Then for each source TGF, the corresponding electron TGF locations are calculated by solving the intersections of the geomagnetic field line going through this source TGF and the orbital plane of instrument, as shown in Figure 3. The lengths of geomagnetic field line from the location at which the TGF is initiated to its detection as an electron TGF on the spacecraft, which is a good indicator of the time history of electron TGFs, are derived as well. Because the TGF rate is correlated to flash rate by the TGF/lightning ratio, the occurrence rate of the electron TGF can be
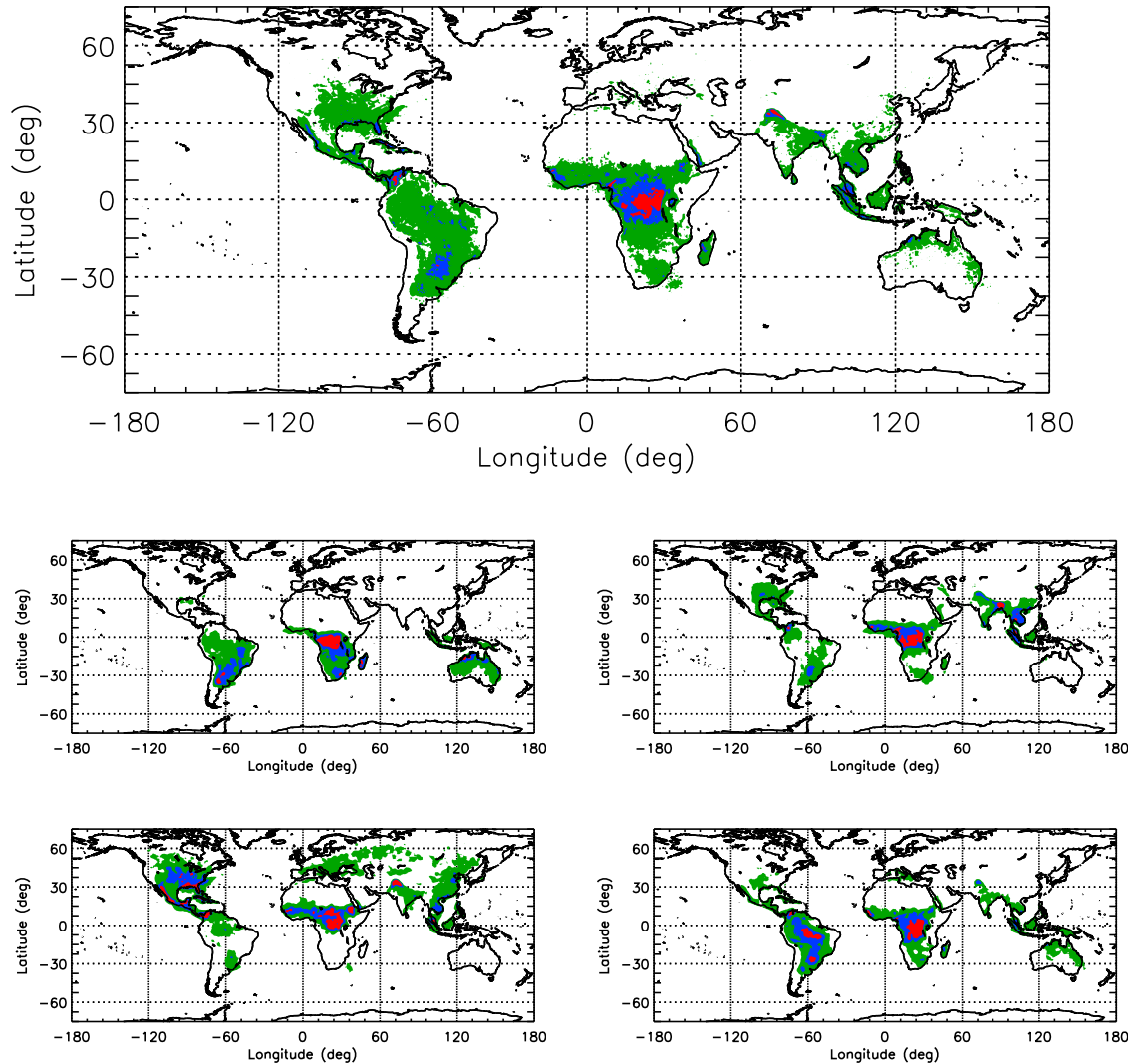
Figure 1. Lightning map by LIS/OTD [*Christian et al.*, 1999; *Boccippio et al.*, 2000]. (top) Full-climatology (full year) map, (middle left) Dec-Jan-Feb season map, (middle right) Mar-Apr-May season map, (bottom left) Jun-Jul-Aug season map, and (bottom right) Sep-Oct-Nov season map. The filled contours correspond to lightning rates of 10–30 (green), 30–50 (blue) and ≥ 50 (red) flashes km^{-2} yr^{-1}.
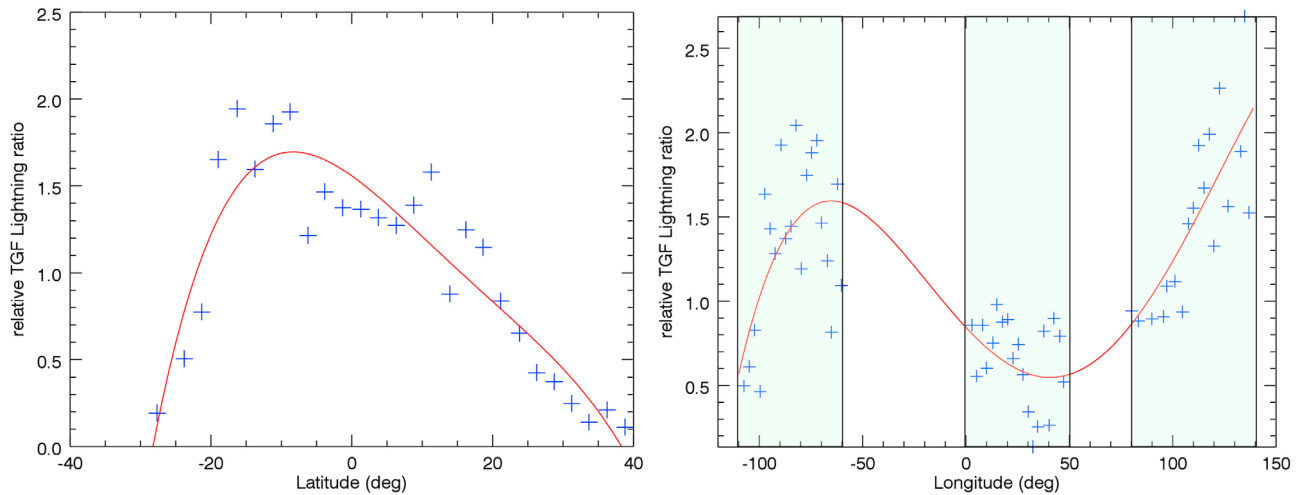
Figure 2. TGF/lightning ratio geographic variation derived from *Smith et al.* [2010, Figures 6 and 7]. For longitude, data only in the continental regions (shadowed areas in Figure 2 (right)) are used because oceanic areas have low flash rates then are not used in creating the electron TGF maps. Data are shown with plus symbols while the fit results (4th degree polynomial) are shown with solid lines.

estimated, it is a relative rate though. Therefore, apart from location, every electron TGF has two more characteristic parameters: relative rate and length of geomagnetic field line.

[15] With these electron TGF locations, we make an electron TGF location map as follows: First, set the pixel size of the map to 2 degree × 2 degree; Second, for each pixel, determine which electron TGF locations fall inside. For each pixel in the electron TGF location map, there are sometimes two groups of electron TGFs which come from the Southern and Northern parts of the Earth, respectively. We take the summed rate of all electron TGFs of the two groups as the rate for that pixel. The length of geomagnetic field line is similar in each group but sometimes greatly different between the two groups. However, we found that the total rate of electron TGFs in one group is 10 times greater than that of the other group for >90% of the valid pixels in the electron TGF location map. Therefore, for simplicity, we take the length of geomagnetic field line of the group with higher rate as the length for that pixel.

[16] Fermi has a nearly circular orbit with a typical altitude of 560 km. The full-year averaged electron TGF prediction map for Fermi GBM is made for this altitude using the full year lightning map, as shown in Figure 4. Seasonal maps are also produced with the corresponding seasonal lightning map, as shown in Figure 5.

[17] In addition, full-year averaged electron TGF location predictions are made for some typical altitudes: 350 km, 470 km, 1000 km, 2000 km and 5000 km, as shown in Figures 6 and 7. These maps could serve as guidelines for potential TGF observations at these altitudes.

5. Discussion and Conclusion

[18] In Figures 4, 5, and 7, we compare the compliance between the locations of electron TGFs that have been detected with BATSE, RHESSI and GBM (see Table 1) and the predicted regions of high electron TGF rates. The detection of electron TGFs by AGILE is strongly hampered by the plastic anti-coincidence shield, which surrounds all the
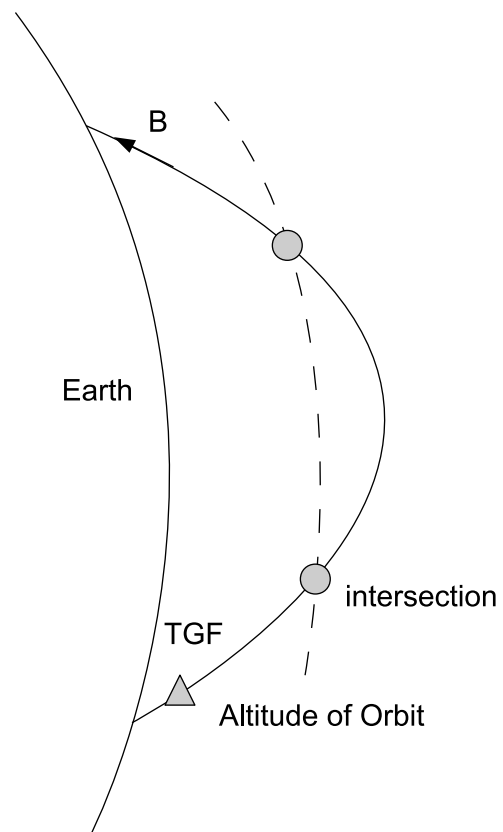

Figure 3. Illustration of tracing the geomagnetic field. The solid line represents a field line that passes through a TGF-produced electrons source (triangle) and the dashed line the altitude of a spacecraft, resulting in two intersections (circles). The altitude of electron production by the TGF is assumed to be 30 km since this is the average altitude of electron generation by Compton scattering and pair production by the primary gamma-rays of TGFs.
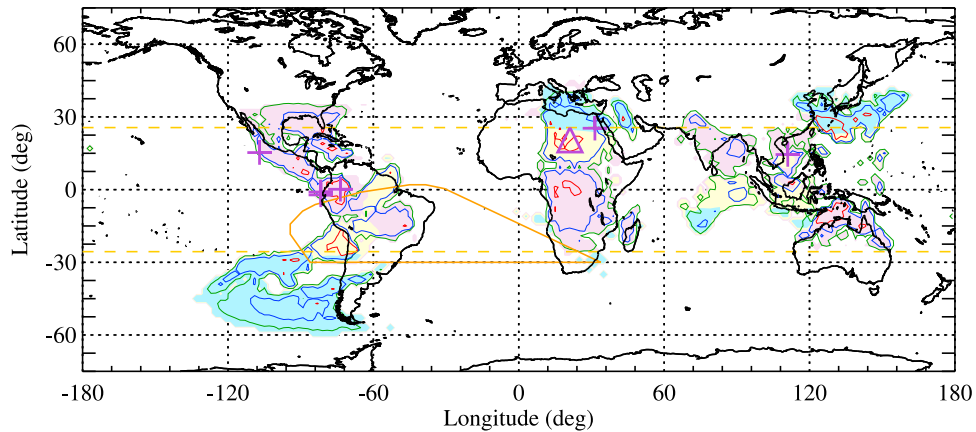
Figure 4. Full-year averaged location map of electron TGFs for GBM (altitude of 560 km). The solid line contours correspond to relative electron TGF rates of 1–5 (green), 5–20 (blue) and ≥ 20 (red). The colored regions indicate the length of the magnetic field line to that point: 500–2000 (light red), 2000–5000 (light yellow) and ≥ 5000 (light blue) km. The solid yellow polygon shows the South Atlantic Anomaly (SAA) region, in which the GBM detectors are turned off, and the dashed yellow lines are the latitude limits of the GBM orbit. The plus symbols indicate the locations of GBM detected electron TGFs, while the triangle is an RHESSI observed electron TGF.
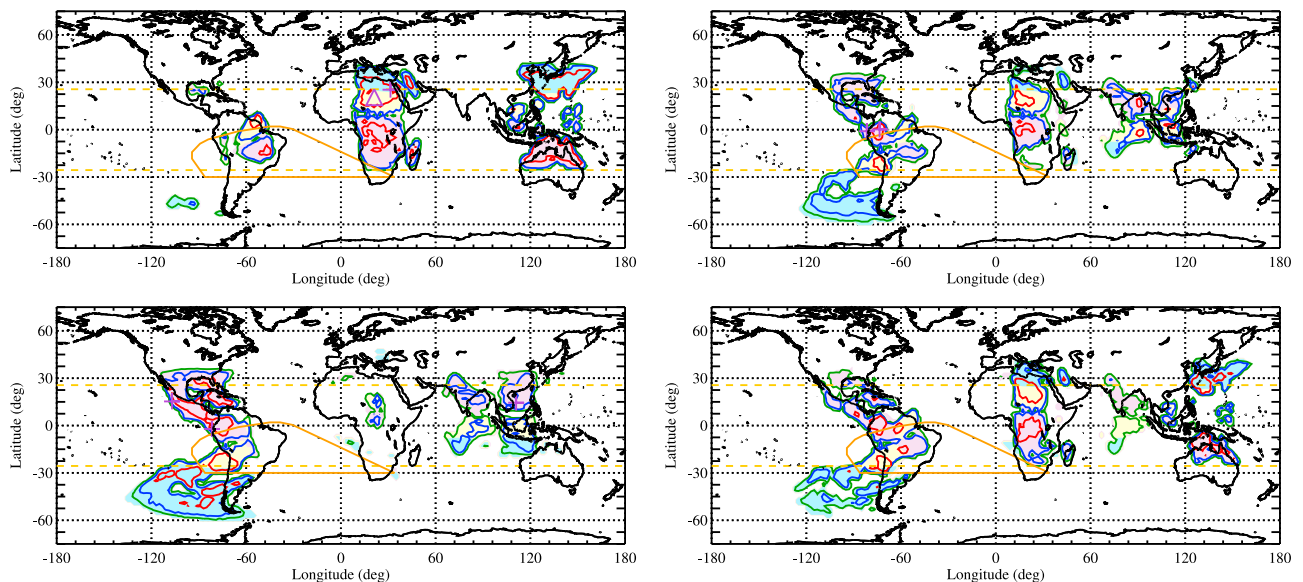
Figure 5. Seasonal location maps of electron TGFs for GBM (altitude of 560 km). (top left) Dec-Jan-Feb season map, (top right) Mar-Apr-May season map. (bottom left) Jun-Jul-Aug season map, and (bottom right) Sep-Oct-Nov season map. The contours, regions, lines and symbols have the same definitions as in Figure 4.
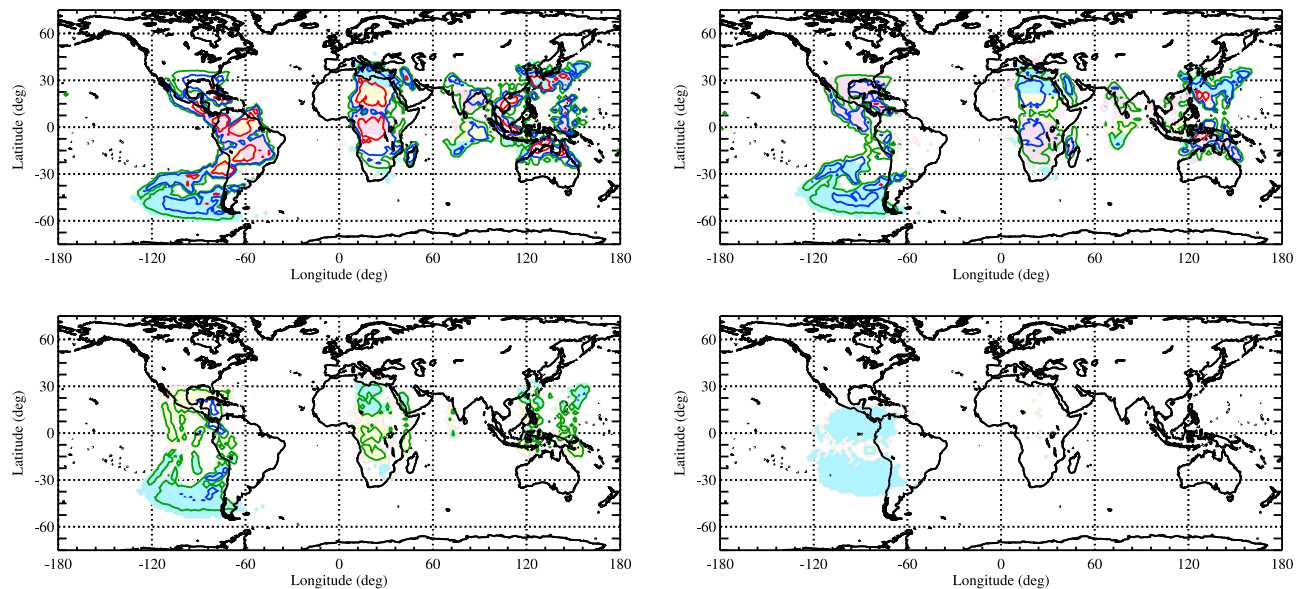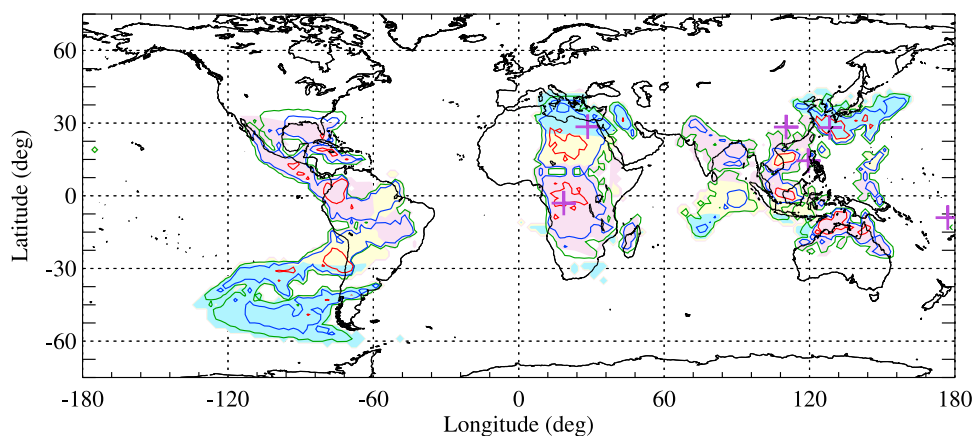
Figure 6. Full-year averaged location maps of electron TGFs for different altitudes. (top left) Altitude of 350 km, (top right) altitude of 1000 km, (bottom left) altitude of 2000 km, and (bottom right) altitude of 5000 km. The contours and regions have the same definitions as in Figure 4.

payload except the interface with the spacecraft and is designed for charged particle rejection (M. Marisaldi, private communication, 2011). Table 1 includes the six GBM TGFs that can be confidently classified as electron TGFs, out of the 172 TGFs detected by the GBM flight software through the end of July 2011. Classification of a GBM TGF as an electron TGF is based on the event having at least several of the following characteristics: a duration longer than 1 ms (not possibly caused by multiple gamma-ray pulses), the spectrum containing a positron annihilation line (511 keV), a spectrum with a lower maximum energy, radio observations from WWLLN showing lightning at a magnetic footpoint but not underneath Fermi, and having signal only in detectors on one side of the spacecraft. The BATSE electron TGFs are those identified by *Dwyer et al.* [2008] based upon differing time histories in the eight BATSE detectors. The RHESSI event has a distinctive time history with a mirror peak [*Smith*

et al., 2006]. Since RHESSI's altitude (about 600 km) is close to that of Fermi (560 km), location predictions for RHESSI and Fermi GBM will be similar and we use a single map for these two instruments.

[19] With a single exception, all known electron TGFs are within the predicted high-rate regions. If we compare the seasonal maps (Figure 5) to the full-year averaged map (Figure 4), the seasonal maps show an improvement in the agreement of the locations of the observed electron TGFs with the predicted high-rate regions. For example, the GBM events in North Africa are out of the red line in Figure 4 but well inside the red line in Figure 5. A significant improvement for the GBM events in North America is also evident. Although duration is not only determined by the propagation effect, a good correlation between duration and predicted length of magnetic field line is found, see Table 1. The locations of electron TGFs matching the predicted high-rate

Figure 7. Full-year averaged location map of electron TGFs for BATSE (altitude of 470 km). The contours and regions have the same definitions as in Figure 4, and the plus symbols indicate the locations of electron TGFs detected by BATSE [*Dwyer et al.*, 2008].

Table 1. Electron TGFs Detected by GBM, RHESSI (D. M. Smith, Private Communication, 2011) and BATSE [*Dwyer et al.*, 2008][a]

Instrument	Identifier	Date (yymmdd)	Longitude (deg)	Latitude (deg)	Duration (ms)	B Field Line Length (km)
GBM	080807.357	080807	253.01	15.30	2.5	764
GBM	090813.215	090813	278.29	−2.19	4	1198
GBM	091214.495	091214	31.42	25.34	30	5493
GBM	100515.316	100515	278.29	−0.98	5	1124
GBM	110410.216	110410	286.38	0.15	2.2	1125
GBM	110625.474	110625	111.01	14.47	6	1216
RHESSI	–	040117	21.119	20.535	30	3797
BATSE	01470	920309	128.31	28.18	20	6371
BATSE	02221	930305	28.44	28.46	25	6294
BATSE	02248	930315	18.58	−3.03	<10	720
BATSE	02457	930723	110.33	28.37	4	620
BATSE	07208	981111	119.44	14.45	1.5	1095
BATSE	07229	981125	177.04	−9.03	2	867

[a]The altitudes of GBM, RHESSI and BATSE are 560 km, 578 km and 470 km, respectively. For the purpose of comparison with the magnetic field line length, durations are estimated from their light curves. For BATSE TGF 02248, high resolution data is not available so a range is given.

regions, especially the enhancement from full-year averaged map to seasonal maps, and the time history correctly reflecting the predicted magnetic field line length, demonstrate the validity of our calculation.

[20] As the only exception, BATSE TGF 07229 occurred when the Compton Observatory was over the Pacific (Table 1) outside the areas where electron TGFs are probable according to our analysis. Occasionally electron TGFs will trace back to lightning in regions of lower lightning rates. The southern magnetic footprint of this TGF is near the islands of Fiji and Vanu Levu, with a closest approach to land of ~250 km. While the lightning rate at the precise footprint location is only 1.44 flashes $km^{-2}yr^{-1}$ for the season, the rate reaches 2.61 flashes year $km^{-2} yr^{-1}$ within 200 km and 4.72 flashes year $km^{-2} yr^{-1}$ at Fiji, 360 km away. The higher rates suggest that the source might be farther from the calculated footprint than expected.

[21] A thunderstorm can typically produce both close and distant electron TGFs, from the two intersections shown in Figure 3. The close solutions produce electron TGF regions that are similar to the parent lightning activity regions, and to the geographic distribution of gamma-ray TGFs from that lightning. In some cases the distant solutions create regions of high rates of electron TGFs that are above areas of low lightning activity; gamma-ray TGFs will rarely be detected above these areas. Examples of such regions (Figure 4) include northern Africa, sections of the Pacific off the west coast of South America and the south coast of Japan, and a portion of the Indian Ocean. Indeed, while gamma-ray TGFs are extremely rare above +15° latitude in Africa, two distinctive electron TGFs with double peaks from magnetic mirroring have been observed over Northern Africa, one by RHESSI on 17 January 2004 [*Smith et al.*, 2006], and the second by GBM on 14 December 2009 [*Briggs et al.*, 2011] (Table 1). These areas are well suited for observations of the emissions (e.g. optical emissions, secondary ionization and gamma-rays [*Lehtinen et al.*, 2001]) by the relativistic particles interacting with the upper atmosphere at the conjugate point to the source since there may be less other activity.

[22] In order to determine which altitude range is best for electron TGF observation instruments, we integrate the electron TGF rates over the predicted maps for various altitudes, with each pixel weighted for its geometrical area. In this way, we derive the relative number of electron TGFs per year, which we use as the figure of merit (as shown in

Figure 8). It clearly shows that the best altitude range is within ≈1000 km, and that lower is better. However, this is only a rough scale for comparison since instruments may have different inclination angles (exposure time), detection thresholds, and other instrumental effects. Those factors will affect the number of actually observed electron TGFs.

[23] As part of calculating the detection probabilities of electron TGFs, *Carlson et al.* [2011] calculated a map of electron TGF detection probability for GBM, accounting for exposure. Another difference is that the TGF sources used are the observed RHESSI TGF sample, which doesn't suffer from the variations of the TGF/lightning ratio of our method, but has different observational biases, such as variations in the RHESSI observing time, data collection, background and TGF detection sensitivity.

[24] Although we correct the TGF/lightning ratio variation in latitude and longitude using RHESSI data, the TGF/lightning ratio may have more complicated geographic and seasonal dependencies, which are not accounted for in our prediction. Moreover, it would be useful to calculate the absolute rate of electron TGFs if the absolute value of TGF/lightning ratio were to be well established globally. Finally, the contribution of electron TGFs to the population of electrons and positrons in the inner radiation belt is an interesting
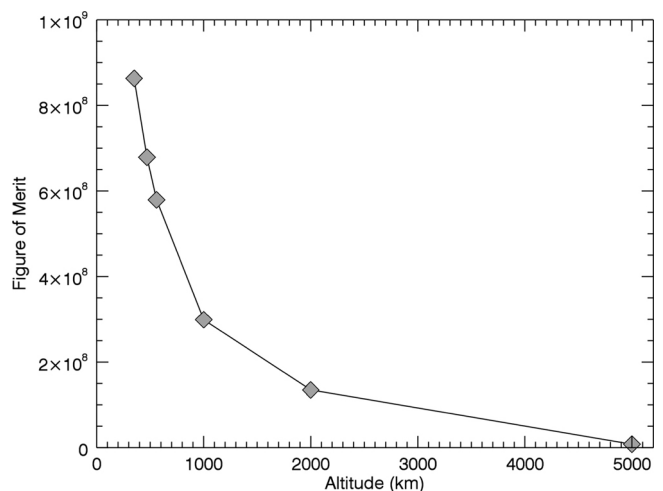
Figure 8. Figure of merit for various altitudes: 350, 470, 560, 1000, 2000, 5000 (km).

issue. A more complex and model-dependent approach is needed to address this problem, requiring knowledge of the intensity distribution of electron TGFs and assumptions about the fraction of electrons scattered out of the beam.

[25] Although the geomagnetic field changes with time, the IGRF-11 model predicts a shift at 560 km altitude of less than 1 degree within 10 years so our calculations are useful for near past and future observations.

References

Boccippio, D. J., W. Koshak, R. Blakeslee, K. Driscoll, D. Mach, D. Buechler, W. Boeck, H. J. Christian, and S. J. Goodman (2000), The optical transient detector (OTD): Instrument characteristics and cross-sensor validation, *J. Atmos. Oceanic Technol.*, 17(4), 441–458, doi:10.1175/1520-0426(2000)017<0441:TOTDOI>2.0.CO;2.

Briggs, M. S., et al. (2010), First results on terrestrial gamma ray flashes from the Fermi Gamma-ray Burst Monitor, *J. Geophys. Res.*, 115, A07323, doi:10.1029/2009JA015242.

Briggs, M. S., et al. (2011), Electron-positron beams from terrestrial lightning observed with Fermi GBM, *Geophys. Res. Lett.*, 38, L02808, doi:10.1029/2010GL046259.

Carlson, B. E., N. G. Lehtinen, and U. S. Inan (2007), Constraints on terrestrial gamma ray flash production from satellite observation, *Geophys. Res. Lett.*, 34, L08809, doi:10.1029/2006GL029229.

Carlson, B. E., N. G. Lehtinen, and U. S. Inan (2009), Observations of terrestrial gamma-ray flash electrons, *AIP Conf. Proc.*, 1118(1), 84–91, doi:10.1063/1.3137717.

Carlson, B. E., T. Gjesteland, and N. Østgaard (2011), Terrestrial gamma-ray flash electron beam geometry, fluence, and detection frequency, *J. Geophys. Res.*, 116, A11217, doi:10.1029/2011JA016812.

Christian, H. J., et al. (1999), The lightning imaging sensor, paper presented at the 11th International Conference on Atmospheric Electricity, NASA, Guntersville, Ala.

Cohen, M. B., U. S. Inan, and G. Fishman (2006), Terrestrial gamma ray flashes observed aboard the Compton Gamma Ray Observatory/Burst and Transient Source Experiment and ELF/VLF radio atmospherics, *J. Geophys. Res.*, 111, D24109, doi:10.1029/2005JD006987.

Cohen, M. B., U. S. Inan, R. K. Said, M. S. Briggs, G. J. Fishman, V. Connaughton, and S. A. Cummer (2010), A lightning discharge producing a beam of relativistic electrons into space, *Geophys. Res. Lett.*, 37, L18806, doi:10.1029/2010GL044481.

Connaughton, V., et al. (2010), Associations between Fermi Gamma-ray Burst Monitor terrestrial gamma ray flashes and sferics from the World Wide Lightning Location Network, *J. Geophys. Res.*, 115, A12307, doi:10.1029/2010JA015681.

Cummer, S. A., Y. Zhai, W. Hu, D. M. Smith, L. I. Lopez, and M. A. Stanley (2005), Measurements and implications of the relationship between lightning and terrestrial gamma ray flashes, *Geophys. Res. Lett.*, 32, L08811, doi:10.1029/2005GL022778.

Dwyer, J. R. (2003), A fundamental limit on electric fields in air, *Geophys. Res. Lett.*, 30(20), 2055, doi:10.1029/2003GL017781.

Dwyer, J. R. (2007), Relativistic breakdown in planetary atmospheres, *Phys. Plasmas*, 14(4), 042901, doi:10.1063/1.2709652.

Dwyer, J. R., and D. M. Smith (2005), A comparison between Monte Carlo simulations of runaway breakdown and terrestrial gamma-ray flash observations, *Geophys. Res. Lett.*, 32, L22804, doi:10.1029/2005GL023848.

Dwyer, J. R., B. W. Grefenstette, and D. M. Smith (2008), High-energy electron beams launched into space by thunderstorms, *Geophys. Res. Lett.*, 35, L02815, doi:10.1029/2007GL032430.

Finlay, C. C., et al. (2010), International Geomagnetic Reference Field: The eleventh generation, *Geophys. J. Int.*, 183(3), 1216–1230, doi:10.1111/j.1365-246X.2010.04804.x.

Fishman, G. J., et al. (1994), Discovery of intense gamma-ray flashes of atmospheric origin, *Science*, 264(5163), 1313–1316, doi:10.1126/science.264.5163.1313.

Fishman, G. J., et al. (2011), Temporal properties of the terrestrial gamma-ray flashes from the Gamma-Ray Burst Monitor on the Fermi Observatory, *J. Geophys. Res.*, 116, A07304, doi:10.1029/2010JA016084.

Fuschino, F., et al. (2011), High spatial resolution correlation of AGILE TGFs and global lightning activity above the equatorial belt, *Geophys. Res. Lett.*, 38, L14806, doi:10.1029/2011GL047817.

Grefenstette, B. W., D. M. Smith, B. J. Hazelton, and L. I. Lopez (2009), First RHESSI terrestrial gamma ray flash catalog, *J. Geophys. Res.*, 114, A02314, doi:10.1029/2008JA013721.

Gurevich, A. V., G. M. Milikh, and R. Roussel-Dupre (1992), Runaway electron mechanism of air breakdown and preconditioning during a thunderstorm, *Phys. Lett. A*, 165(5–6), 463–468, doi:10.1016/0375-9601(92)90348-P.

Inan, U. S., S. C. Reising, G. J. Fishman, and J. M. Horack (1996), On the association of terrestrial gamma-ray bursts with lightning and implications for sprites, *Geophys. Res. Lett.*, 23(9), 1017–1020, doi:10.1029/96GL00746.

Lehtinen, N. G., T. F. Bell, and U. S. Inan (1999), Monte Carlo simulation of runaway MeV electron breakdown with application to red sprites and terrestrial gamma ray flashes, *J. Geophys. Res.*, 104(A11), 24,699–24,712, doi:199910.1029/1999JA900335.

Lehtinen, N. G., U. S. Inan, and T. F. Bell (2001), Effects of thunderstorm-driven runaway electrons in the conjugate hemisphere: Purple sprites, ionization enhancements, and gamma rays, *J. Geophys. Res.*, 106(A12), 28,841–28,856, doi:200110.1029/2000JA000160.

Marisaldi, M., et al. (2010), Detection of terrestrial gamma ray flashes up to 40 MeV by the AGILE satellite, *J. Geophys. Res.*, 115, A00E13, doi:10.1029/2009JA014502.

Meegan, C., et al. (2009), The Fermi gamma-ray burst monitor, *Astrophys. J.*, 702, 791–804.

Roussel-Dupré, R., and A. V. Gurevich (1996), On runaway breakdown and upward propagating discharges, *J. Geophys. Res.*, 101(A2), 2297–2311, doi:199610.1029/95JA03278.

Smith, D. M., L. I. Lopez, R. P. Lin, and C. P. Barrington-Leigh (2005), Terrestrial gamma-ray flashes observed up to 20 MeV, *Science*, 307(5712), 1085–1088, doi:10.1126/science.1107466.

Smith, D. M., et al. (2006), The anomalous terrestrial gamma-ray flash of 17 January 2004, *Eos Trans. AGU*, 87(52), Fall Meet. Suppl., Abstract AE31A-1040.

Smith, D. M., B. J. Hazelton, B. W. Grefenstette, J. R. Dwyer, R. H. Holzworth, and E. H. Lay (2010), Terrestrial gamma ray flashes correlated to storm phase and tropopause height, *J. Geophys. Res.*, 115, A00E49, doi:10.1029/2009JA014853.

Tavani, M., et al. (2011), Terrestrial gamma-ray flashes as powerful particle accelerators, *Phys. Rev. Lett.*, 106(1), 018501, doi:10.1103/PhysRevLett.106.018501.

M. S. Briggs, V. Connaughton, S. Guiriec, and S. Xiong, NSSTC, 320 Sparkman Drive, Huntsville, AL 35805, USA. (shaolin.xiong@uah.edu)

G. J. Fishman, Space Science Office, NASA Marshall Space Flight Center, VP62, Huntsville, AL 35812, USA.

G. Fitzpatrick and D. Tierney, School of Physics, University College Dublin, Belfield, Stillorgan Road, Dublin 4, Ireland.

S. Foley, Max-Planck-Institut für Extraterrestrische Physik, Giessenbachstr. 1, D-85748 Garching, Germany.

R. H. Holzworth and M. L. Hutchins, Earth and Space Sciences, University of Washington, Seattle, WA 98195, USA.